

1SWASP J074658.62+224448.5: A LOW MASS-RATIO CONTACT BINARY AT THE PERIOD CUTOFF

L.-Q. JIANG^{1,2,3}, S.-B. QIAN^{1,2,3}, J. ZHANG^{1,2,3}, AND X. ZHOU^{1,2,3}¹ Yunnan Observatories, Chinese Academy of Sciences, P.O. Box 110, 650011 Kunming, China; linqiao@ynao.ac.cn² Key Laboratory of the Structure and Evolution of Celestial Objects, Chinese Academy of Sciences, P.O. Box 110, 650011 Kunming, China³ Graduate University of the Chinese Academy of Sciences, Yuquan Road 19, Sijingshang Block, 100049 Beijing City, China

Received 2014 October 4; accepted 2015 March 6; published 2015 April 28

ABSTRACT

The first sets of high-quality light curves of the extremely short period eclipsing binary 1SWASP J074658.62+224448.5 (hereafter J074658) were obtained in 2012 and 2014. The photometric solutions were derived using the 2013 version of the Wilson–Devinney code. Two different modes of overcontact binaries were used to analyze the light curves, and the adopted solutions show that J074658 is a shallow contact system (the degree of contact is $f = 13.1 \pm 2.1\%$) with a mass ratio of $q = 0.386 \pm 0.017$. The two components have very close temperatures, which may indicate that J074658 is in thermal contact. The variation of the orbital period was studied using all the available times of minimum light. According to the $O - C$ diagram, the orbital period of J074658 shows an increase at a rate of $\dot{P} = 5.39 \times 10^{-7}$ days yr⁻¹ in about an eight-year span. The reasons for the period increase compared with other well-studied contact binaries with extremely short periods are discussed. The period increase may be caused by mass transfer from the less massive component to the more massive one, or it could be only part of a long period cyclic variation that may reveal the presence of a third body. In this paper, the latter is suggested.

Key words: binaries: close – binaries: eclipsing – stars: evolution – stars: individual (1SWASP J074658.62+224448.5)

1. INTRODUCTION

It is well known that W UMa type contact binaries have a very sharp period cutoff at about 0.22 days, although the reasons for this period cutoff are far from clear. Although there are several theories (Rucinski 1992; Stepień 2006; Stepień 2011; Jiang et al. 2012) that try to explain the observed short-period cutoff, the largest obstacle is the apparent lack of this kind of system. Thanks to surveys such as SDSS, the WFCAM Transit Survey, and SuperWASP (Becker et al. 2011; Norton et al. 2011; Nefs et al. 2012; Lohr et al. 2013a), many short-period eclipsing binary candidates can now be discovered and investigated in detail. The increasing number of close binaries at the short-period limit provides us a chance to study the reasons for the sharp period cutoff.

The system J074658 was discovered as a short-period ($P = 0.22085$ days) eclipsing binary candidate by Norton et al. (2011), with a maximum $V_{\text{mag}} = 14.06$ and depths of the primary and secondary minima of 0.53 and 0.46 mag, respectively. Soon afterward, Lohr et al. (2012) presented the results of a search for period changes in 53 candidates, and a period ($P = 19081.403$ s) identical to that found in Norton et al. (2011) was obtained. The system was later investigated again by Lohr et al. (2013a), who used an improved period change detection method to search for period changes in the eclipsing systems with periods below 2000 s. Possibly due to the time span of the data not being long enough (~ 4 yr), there was still no any significant change detected by Lohr et al. (2013a). In this paper, the first high-precision charge-coupled device (CCD) light curves are presented and analyzed. Then, the period changes are studied and discussed.

2. OBSERVATION AND DATA REDUCTION

Nine photometric observations of J074658 were carried out from 2012 to 2014, including three light curve observations and six minimum light observations, using several telescopes

in China. The detailed observation log is given in Table 1. On all the observing nights, bias and flat-field images were obtained for use in preprocessing. All the CCD images were processed with the DAOPHOT package of IRAF in a standard mode. Differential magnitudes were then determined. In order to get better light curves, the fluxes of two stars (GSC1912-1105, GSC1912-1015) were summed together into one comparison star, and their differential magnitudes were determined to verify that the two comparison stars are invariable. The coordinates and visual magnitudes of the variable star and the two comparison stars are listed in Table 2.

The five phased light curves are displayed in Figure 1 and the seven minimum light curves are displayed in Figure 2. The phases were calculated with the new revised period of 0.22085007 days (for details see Equation (2)). As shown in Figure 1, the five light curves are typical EW-type with a small difference in the depths of the primary and secondary. The two sets of light curves in 2012 December and 2014 November almost coincide with each other in both the R_c and I_c bands. We note that the large scatter points between phase 0.55 and phase 0.75 in 2012 November (in red) are due to cloudy weather during the observation. For the light curve in 2014 January (in blue), a slight asymmetry, i.e., the primary maxima (at phase 0.25) are higher than the secondary ones, as can be seen. As in the case of other contact binaries of this type, such as CC Com, 1SWASP J160156.04+202821.6, NSVS4484038, and 1SWASP J133105.91+121538.0 (Köse et al. 2011; Elkhateeb et al. 2014; Essam et al. 2014; Zhang et al. 2014), a deep convective envelope along with fast rotation can produce a strong magnetic dynamo and solar-like activity, including photospheric dark spots (Qian et al. 2013). Therefore, this asymmetry may be caused by spot activity on the surface of the components. In addition, the blue light curve seems to be translated upward relative to the others, which is probably caused by a magnitude shift of the comparison stars over the months, which can be seen in the lower straight blue light

Table 1
Observational Log of J074658

Date	Filters and Integration time	Telescopes	Field	Numbers	Type
2012 Dec 25	R_c 20 s I_c 20 s	1 m	$7/3 \times 7/3$	418 groups	light curve
2013 Feb 25	N 20 s	1 m	$7/3 \times 7/3$	261 frames	minimum light
2014 Jan 09	R_c 40 s	2.16 m	$9' \times 9'$	362 frames	light curve
2014 Jan 10	N 50 s	1 m	$7/3 \times 7/3$	126 frames	minimum light
2014 Feb 08	V 30 s R_c 15 s I_c 10 s	1 m	$7/3 \times 7/3$	70 groups	minimum light
2014 Nov 08	R_c 15 s I_c 12 s	85 cm	$38' \times 38'$	537 groups	light curve
2014 Nov 08	N 60 s	60 cm	$12/5 \times 12/5$	145 frames	minimum light
2014 Nov 14	N 40 s	1 m	$7/3 \times 7/3$	122 frames	minimum light
2015 Feb 08	N 60 s	60 cm	$12/5 \times 12/5$	116 frames	minimum light

Notes. “N” in the second column refers to when no filters were used. In the third column, 1 m and 60 cm refer to the 1.0 m reflecting telescope and the 60 cm Cassegrain reflecting telescope at Yunnan Observatory, both were equipped with an Andor DW436 2k CCD; 85 cm refers to the 85 cm reflecting telescope at the Xinglong station of the National Astronomical Observatories of China, which was equipped with an Andor Tech 2 K CCD; 2.16 m refers to the 2.16 m telescope located in the same place as the 85 cm; this telescope was equipped with a PI 1274 \times 1152 TE CCD55-30-1-348.

Table 2
Information on the Variable and Comparison Stars

Targets	α_{2000}	δ_{2000}	V_{mag}
J074658	$07^{\text{h}}46^{\text{m}}58^{\text{s}}.62$	$+22^{\circ}44'48''.5$	14.30 mag
GSC1912-1105	$07^{\text{h}}46^{\text{m}}48^{\text{s}}.39$	$+22^{\circ}45'07''.8$	14.82 mag
GSC1912-1015	$07^{\text{h}}46^{\text{m}}46^{\text{s}}.05$	$+22^{\circ}44'46''.4$	13.28 mag

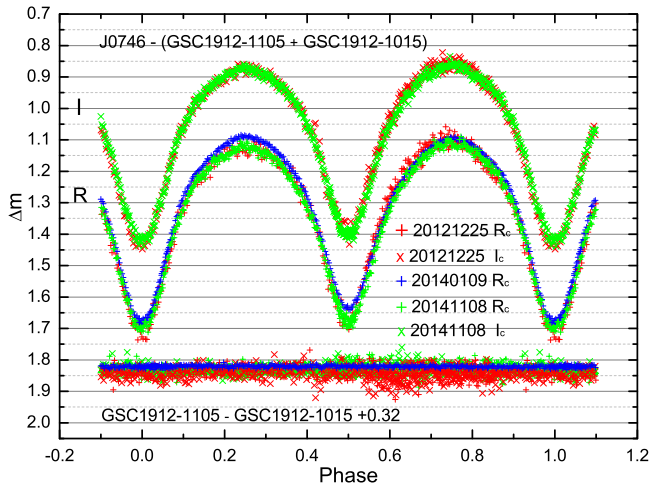


Figure 1. Phased light curves of J074658. Different colors represent light curves observed in different seasons. The pluses refer to light curves in the R_c band, and the crosses refer to light curves in the I_c band. The typical photometric errors for each season of observation are 0.009–0.015 mag in 2012 December, 0.001–0.003 mag in 2014 January, and 0.004–0.009 mag in 2014 November. The magnitude differences between the two comparison stars are also shown in the lower part.

curve. However, the translation does not alter the shape of the light curves, and so does not affect the following analysis.

3. THE ORBITAL PERIOD VARIATIONS

Since no times of minimum light of the system J074658 had been published before, several times of minimum light were derived to investigate the period variations. Base on all of our observations, which are shown in Figures 1 and 2, a least-squares parabolic fitting method was used to determine the times of minimum light, which are listed in Table 3. The time standard used for the data is Heliocentric Julian Dates (HJDs). In order to study the changes in the orbital period of J074658,

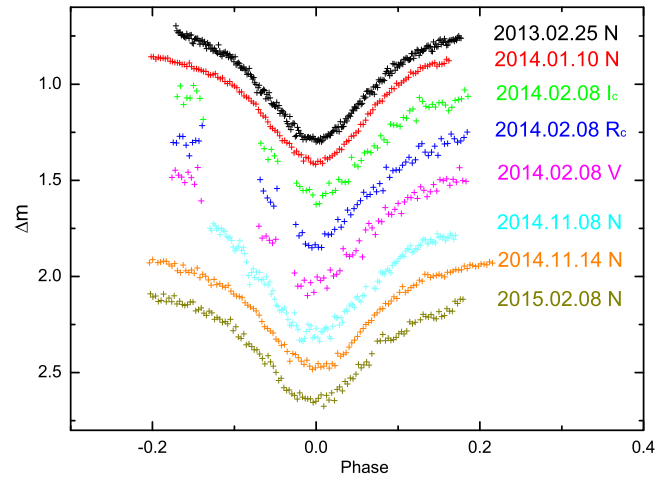


Figure 2. Minimum curves of J074658. Different colors represent curves observed in different seasons. The curves were shifted in magnitude to be shown in one figure.

Table 3
New Times of Minimum Light of J074658

HJD	Errors	Min.	Filter
2456287.210113	0.000468	I	$R_c I_c$ mean
2456287.320238	0.000251	II	$R_c I_c$ mean
2456349.048424	0.000145	I	N
2456667.074173	0.000230	I	R_c
2456667.184800	0.000085	II	R_c
2456667.295092	0.000050	I	R_c
2456668.178214	0.000157	I	N
2456697.110134	0.000539	I	$VR_c I_c$ mean
2456970.304709	0.000198	I	$R_c I_c$ mean
2456970.194535	0.000186	II	$R_c I_c$ mean
2456970.304423	0.000275	I	N
2456976.267617	0.000190	I	N
2457062.069491	0.000311	I	N

Notes. I and II refer to the primary minimum and secondary minimum, respectively.

the eclipse timings in the SuperWASP archive have been collected; these cover a time span from 2006 to 2010. SuperWASP can only detect objects brighter than $V_{\text{mag}} \sim 15$ (Pollacco et al. 2006); while the system has a maximum

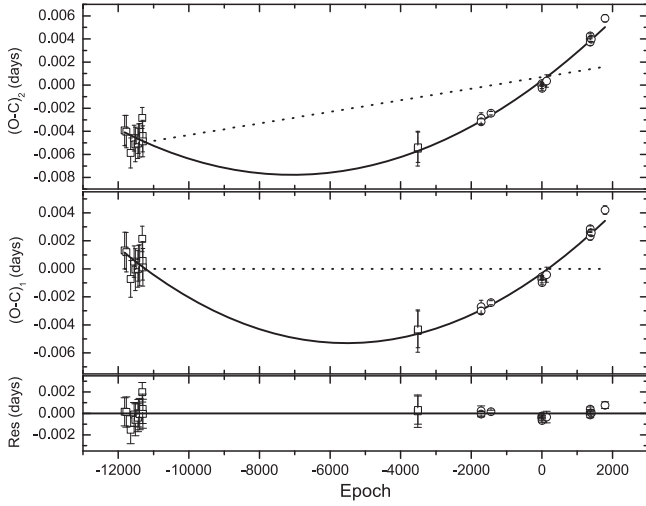


Figure 3. $(O - C)_1$ diagram of J074658 calculated with the linear ephemeris of Equation (1). The $(O - C)_2$ diagram was calculated with the linear ephemeris of Equation (2). Open squares and circles refer to SuperWASP data and our observations, respectively.

$V_{\text{mag}} \approx 14$, it is near the magnitude limit of what SuperWASP can detect. Consequently, the uncertainties on the SuperWASP light curve data points are quite large in comparison with the light curve amplitude, making it hard to measure precise times of minimum. Considering the credibility of the data, eclipse timings in the SuperWASP archive with uncertainties larger than 0.002 days were not used in the analysis of the orbital period.

First, using the following linear ephemeris,

$$\text{Min } I = 2456667.295092 + 0.22084957 \text{ days} \times E, \quad (1)$$

the $(O - C)_1$ values for all timings were computed, and the corresponding $(O - C)_1$ curve is plotted in the upper panel of Figure 3. The initial epoch (Equation (1)) is one of the eclipse timings listed in Table 3, and the adopted period was determined by Lohr et al. (2013a). As shown in the upper panel of Figure 3, the dotted line refers to the revised ephemeris as below,

$$\begin{aligned} \text{Min } I &= 2456667.295791 (\pm 0.00058) \\ &+ 0.22085007 (\pm 0.00000008) \text{ days} \times E, \quad (2) \end{aligned}$$

where 2456667.295791 and $0^{\text{d}}.22085007$ are the revised initial epoch and orbital period, respectively. Then, using this revised ephemeris of Equation (2), the $(O - C)_2$ values for all timings were computed and the corresponding $(O - C)_2$ curve is plotted in the middle panel of Figure 3. As shown in the middle panel of Figure 3, the $(O - C)_2$ curve shows a clearly upward parabola variation, which indicates that the period is continuously increasing. The least-squares solution yields the following ephemeris:

$$\begin{aligned} \text{Min } I &= 2456667.29548 (\pm 0.00016) \\ &+ 0^{\text{d}}.22085188 (\pm 0.00000011) \text{ days} \times E \\ &+ 1.63 (\pm 0.10) \times 10^{-10} \times E^2. \quad (3) \end{aligned}$$

With the coefficient of this square term, a period increase rate of $dP/dt = 5.39 (\pm 0.32) \times 10^{-7} \text{ days yr}^{-1}$ is derived.

The orbital period of J074658 shows an apparently increasing trend. However, we tend to think that this may be part of the cyclic variation, which is due to the light time effect of a third body, based on the following reasons: (1) the observational time span is just 8 yr, so the conclusion of the secular increase in period is premature, (2) the period change rate is $+5.39 (\pm 0.32) \times 10^{-7} \text{ days yr}^{-1}$, which corresponds to a very large mass transfer rate, which may be physically impossible, and (3) the third body may play an important role in the origin and evolution of this kind of system (which will be discussed later).

4. PHOTOMETRIC SOLUTIONS

The three sets of light curves were analyzed together simultaneously and yielded one set of solutions that will reflect more reliable intrinsic features (such as mass ratio, inclination, radius, separation, etc.) than if only one set of light curves is used. The five light curves of J074658 were analyzed using the 2013 version of the W-D program (Wilson & Devinney 1971; Wilson et al. 2010; Wilson 1979, 1990, 2008, 2012; Van Hamme & Wilson 2007). Because systems with very short periods are always expected to be relatively low in mass and late in spectral type, their lights are mainly radiated in the R and I bands. So we used the USNO-B1 Catalog measurements of $\bar{R} = 14.235$ with a color index of $\bar{R} - I = 0.755$ and the SDSS-DR7 photometry of $R = 13.97$ with a color index of $R - I = 0.54$ from the VizieR database (Ochsenbein et al. 2000) to estimate the effective temperature of J074658, which corresponds to a spectral type of about $K4 - K7$ (Cox 2000). Thus, the temperature of the primary star was estimated to be in a range from 4000 to 4600 K. During the analysis, the following atmospheric parameters were adopted: the bolometric albedos $A_1 = A_2 = 0.5$ and the gravity-darkening coefficients $g_1 = g_2 = 0.32$, which correspond to the common convective envelope of both components; for the bolometric and bandpass limb-darkening coefficients, an internal computation with the logarithmic law were used. Different modes (Modes 1–5 correspond to overcontact with more constraints, detached, overcontact with fewer constraints, semi-detached with star 1 accurately filling its limiting lobe, and semi-detached with star 2 filling its limiting lobe, respectively) were tried, and the solutions converged at mode 1 and 3.

Since no photometric or spectroscopic solution has been published, and the primary temperature estimated by the color indices should have some degree of uncertainty, we adopted the following processing steps to derive a more reliable solution. The primary temperature was set to vary from 4000 to 4600 K with a step of 100 K, and the mass ratio was set to vary from 0.3 to 3.5 with a step of 0.1; convergent solutions were achieved for each combination of temperature and mass ratio. The relation between the resulting sum of the weighted square deviations Σ and q is plotted in Figure 4, and to increase confidence, the two modes are used separately to find the best-fit solution. As shown in the Figure 4, first, in both mode 1 and mode 3, different lines with different temperatures share a similar shape, and also yield a similar mass ratio of the minimum $\Sigma \text{ res}^2$; the $\Sigma \text{ res}^2$ derived from mode 3 is less than that of mode 1 throughout the whole mass ratio range. Second, the curves in the left panel derived using mode 1 show a relatively sharp minimum point at $q = 0.37$ or $q = 0.38$, where the curves in the right panel derived using mode 3 show a

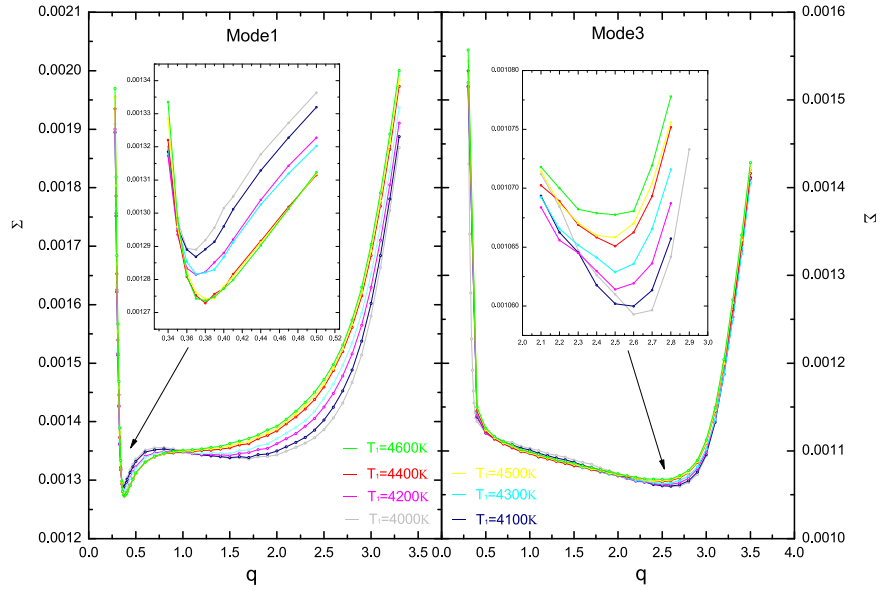


Figure 4. Relations between q and Σ determined by mode 1 and mode 3. Different color lines stand for different primary temperatures.

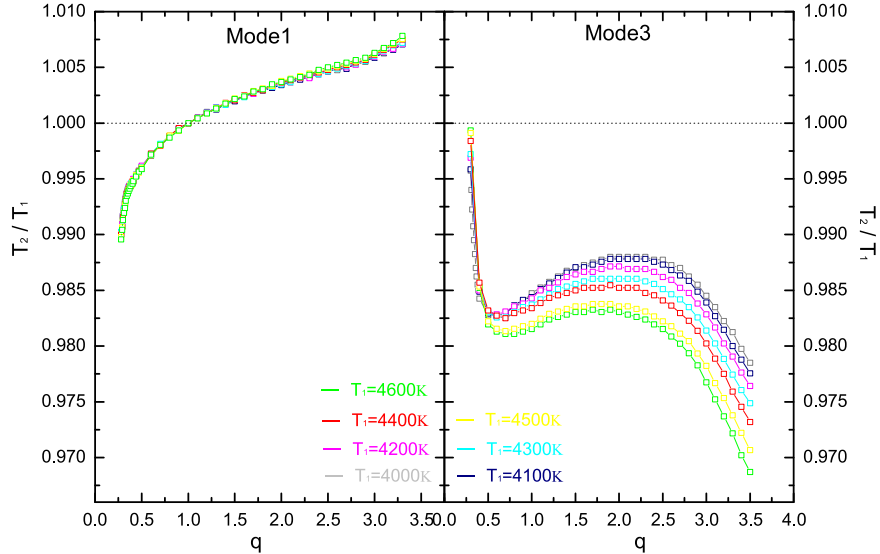


Figure 5. Temperature ratio (T_2/T_1) to mass ratio (q) diagram. Different colored lines refer to different primary temperatures.

poorly defined minimum point at $q = 2.5$ or $q = 2.6$, which is merely the lowest part of a very broad and nearly flat region.

Regardless of the correct mode, according to Wilson’s manual, mode 3 has five more free parameters (g_2 , T_2 , A_2 , x_2 , and y_2) than mode 1, and a fitting mode with more adjustable parameters will give a lower value of Σres^2 than a highly constrained one, of course corresponding to better fits for any contact binary light curves. Furthermore, also mentioned in the manual, the stars in mode 3 can be in geometrical contact without being in thermal contact. Figure 5 shows the relation between the temperature ratio (T_2/T_1) and the mass ratio (q), and as one can see, the temperature ratio is pretty close to 1 throughout the whole mass ratio range, which corresponds to a very small temperature difference between the two components. The exploration of mass ratios yields a low mass ratio for both mode 1 and mode 3, which means the two

components of J074658 have very different masses and radii. Therefore, the system is not only in geometrical contact, but also in thermal contact, which is fit for mode 1.

Based on the discussion above, although mode 3 gives a relatively lower value of Σres^2 and better fits than mode 1, mode 1 was adopted for further analysis. Considering that the primary temperature was estimated to be in a range from 4000 to 4600 K, according to the left panel of Figure 4, the red line stands for the 4400 K primary temperature, which yields a global minimum Σres^2 value of $q = 0.38$. Therefore, the temperature of star 1 was fixed at $T_1 = 4400 \text{ K}$, and the mass ratio was set to be adjustable at an initial value of $q = 0.38$. The final solutions were obtained by performing a series of differential corrections, which were listed in Table 4. As shown in Table 4, the estimates of the adjustable parameter errors are unrealistically small. Therefore, we

Table 4
Photometric Solutions of J074658 Derived by Simultaneously
Determining the Five Light Curves

Parameters	Values	Errors
Mode	1	...
i [°]	78.6	± 0.1
q [m_2/m_1]	0.395	± 0.004
T_1 [K]	4400	Fixed
T_2 [K]	4376	...
$\Omega_1 = \Omega_2$	2.6385	± 0.0090
$L_1/(L_1 + L_2)(R_c)$	0.7048	± 0.0008
$L_1/(L_1 + L_2)(I_c)$	0.7037	± 0.0007
r_1 (pole)	0.4393	± 0.0009
r_1 (side)	0.4703	± 0.0011
r_1 (back)	0.4992	± 0.0011
r_2 (pole)	0.2876	± 0.0039
r_2 (side)	0.3007	± 0.0048
r_2 (back)	0.3376	± 0.0085
The degree of contact(f)	12.6%	$\pm 1.9\%$
$\Sigma \text{ res}^2$	0.0012	...

recalculate the five light curves individually and the solutions are displayed in Table 5. Based on the five sets of different solutions, the mean values of the parameters are calculated as the final solutions, which are listed in the last column of Table 5, with the corresponding scatters as the standard deviations.

As mentioned before, there is a slightly asymmetry in the blue light curve taken in 2014 January, and thus a spot model was used to fit it. The best fit was achieved with a dark spot on the more massive component; the parameters of the dark spot are also listed in Table 5. All corresponding theoretical light curves calculated with the solutions listed in Table 5 are plotted in Figure 6. Figure 7 shows the geometrical structure of J074658 with a dark spot on the more massive component at phase 0.75 in 2014 January.

5. DISCUSSION AND CONCLUSIONS

Based on the five complete light curves, the first photometric solutions for J074658 are obtained with the W-D code. The solutions were resolved using two different overcontact modes. Although mode 3 gives a much better fitting than mode 1, mode 1 gives more convincing results, which is also physically reasonable. Thus, mode 1 is adopted in this paper. Based on all the results, J074658 is a shallow contact binary system with a filling-out factor of about $13.1 \pm 2.1\%$. The photometric solution gives an inclination of $79.0^\circ \pm 0.6^\circ$ and a mass ratio of 0.386 ± 0.017 . The two components have nearly equal surface temperatures in spite of their very different masses and radii, which may indicate that the system is in thermal contact.

The orbital period change of the system is analyzed in this paper. The general $O - C$ trend reveals a period increase at a rate of $5.39(\pm 0.32) \times 10^{-7} \text{ days yr}^{-1}$ (0.047 s yr^{-1}). If this is caused by a mass transfer from the less massive component to the more massive one, considering a spectral type of K7V, the mass of the more massive component was estimated as $M_1 = 0.62M_\odot$ (Cox 2000). According to the derived mass ratio of $q = 0.39$, the mass of the secondary is $M_2 = M_1 \times q = 0.24M_\odot$. By considering a conservative mass transfer equation from M_1 to M_2 ,

$$\dot{P}/P = 3\dot{M}_2(1/M_1 - 1/M_2), \quad (4)$$

the mass transfer rate was determined to be $dM_2/dt = -3.19 \times 10^{-7} M_\odot \text{ yr}^{-1}$ for J074658. This rate of mass transfer appear to be at least an order of magnitude greater than that of other binaries (II Per: Zhu et al. 2009; BV Eri: Qian 2002; UU Lyn: Zhu et al. 2007), which is hardly believable.

It is believed that the period increase is part of the cyclic variation due to the presence of a tertiary component. Table 6 shows all the well-studied contact binaries (with photometric and/or spectroscopic data and periodic analysis) that have a period less than 0.23 days. Most of the contact binaries in the table are in marginal contact. It can be seen that except for CC Com, all the others have experienced very rapid period

Table 5
Photometric Solutions Determined by Separately Calculating the Five Light Curves

Parameters	$R_c(2012.12)$	$I_c(2012.12)$	$R_c(2014.09)$	$R_c(2014.11)$	$I_c(2014.11)$	Mean
Mode	1	1	1	1	1	...
i [°]	79.6(± 0.6)	78.4(± 0.5)	79.6(± 0.2)	78.7(± 0.2)	78.9(± 0.3)	79.0(± 0.6)
q (m_2/m_1)	0.384(± 0.012)	0.404(± 0.017)	0.361(± 0.005)	0.398(± 0.007)	0.381(± 0.007)	0.386(± 0.017)
T_1 [K]	4400	4400	4400	4400	4400	4400
T_2 [K]	4376	4377	4372	4377	4376	4376(± 2)
$\Omega_1 = \Omega_2$	2.6160(± 0.0235)	2.6550(± 0.0328)	2.5606(± 0.0097)	2.6443(± 0.0139)	2.6131(± 0.0137)	2.6178(± 0.0367)
$L_1/(L_1 + L_2)$	0.7106(± 0.0021)	0.6992(± 0.0029)	0.7218(± 0.0008)	0.7034(± 0.0011)	0.7112(± 0.0012)	0.7092(± 0.0086)
r_1 (pole)	0.4415(± 0.0024)	0.4378(± 0.0033)	0.4482(± 0.0011)	0.4387(± 0.0015)	0.4416(± 0.0014)	0.4417(± 0.0039)
r_1 (side)	0.4730(± 0.0029)	0.4686(± 0.0039)	0.4813(± 0.0014)	0.4696(± 0.0019)	0.4730(± 0.0017)	0.4731(± 0.0050)
r_1 (back)	0.5016(± 0.0028)	0.4977(± 0.0037)	0.5101(± 0.0014)	0.4985(± 0.0019)	0.5013(± 0.0017)	0.5018(± 0.0049)
r_2 (pole)	0.2852(± 0.0109)	0.2895(± 0.0144)	0.2823(± 0.0046)	0.2882(± 0.0059)	0.2839(± 0.0062)	0.2858(± 0.0030)
r_2 (side)	0.2981(± 0.0133)	0.3027(± 0.0176)	0.2952(± 0.0057)	0.3013(± 0.0072)	0.2967(± 0.0076)	0.2988(± 0.0031)
r_2 (back)	0.3350(± 0.0238)	0.3399(± 0.0314)	0.3336(± 0.0104)	0.3383(± 0.0127)	0.3330(± 0.0135)	0.3360(± 0.0030)
f	12.3(± 10.0)%	13.2(± 13.3)%	16.6(± 4.4)%	12.6(± 5.7)%	11.0(± 5.9)%	13.1(± 2.1)%
θ_s [°]	138.3(± 2.4)
ψ_s [°]	107.9(± 9.3)
r_s [°]	14.59(± 1.86)
T_s/T	0.8544(± 0.1303)
$\Sigma \text{ res}^2$	0.0030	0.0033	0.0008	0.0011	0.0013	...

Table 6
Sample of Contact Binaries with Periods Less than 0.23 days

Name	Period (days)	Subtype	q (or $1/q$)	f (%)	dP/dt (s yr ⁻¹)	M_3 (M_\odot)	Asym	Reference
CC Com	0.220686	W	0.527	4.4–18	+0.0025 ^a	0.066	Yes	(1)–(7)
GSC 1387-0475	0.217811	A	0.474	76.3	...	~0.47	No	(8), (9)
1SWASPJ234401.81-212229.1	0.213676	W	0.422	1.2	-0.313 ^b	0.7	Yes	(10)–(12)
1SWASP J160156.04+202821.6	0.226529	W	0.67	10	+0.094	...	Yes	(13)
SDSS J001641-000925	0.198561	A	0.62	18–25	-8 ^b	0.144/sin i'	No	(14), (15)
1SWASP J074658.62+224448.5	0.220850	A	0.386	13.2	+0.047	...	Yes	Present paper

Notes. The “Asym” column shows whether noticeable asymmetries were found in their light curves.

References. (1) Linnell & Olson (1989), (2) Shengbang (2001), (3) Yang & Liu (2003), (4) Pribulla et al. (2007), (5) Yang et al. (2009), (6) Zola et al. (2010), (7) Köse et al. (2011), (8) Rucinski & Pribulla (2008), (9) Yang et al. (2010), (10) Lohr et al. (2012), (11) Lohr et al. (2013b), (12) Koen (2014), (13) Lohr et al. (2014), (14) Davenport et al. (2013), (15) Qian et al. (2015).

^a The value is average.

^b The rapid period decrease was subsequently identified as part of a long-term sinusoidal variation.

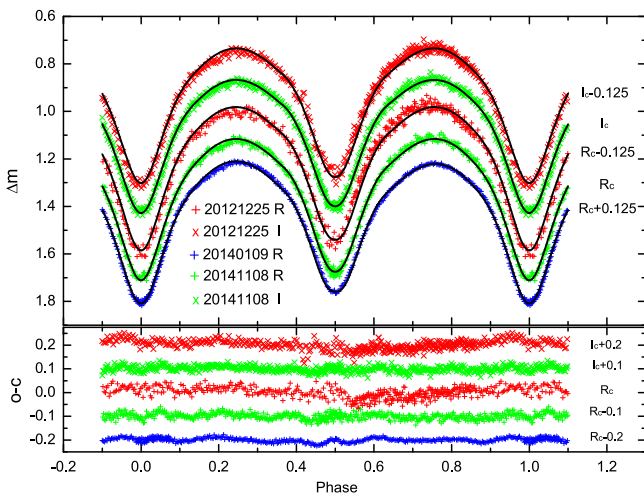


Figure 6. Observed and theoretical light curves (solid line) calculated with the parameters listed in Table 5. Residuals (observed minus calculated light curves) from the solutions are shown in the lower panel.

changes. We should mention that SDSS J001641-000925 was discovered as the first red dwarf contact binary by Davenport et al. (2013), with the orbital period detected to be decreasing rapidly at a rate of $\dot{P} \sim 8 \text{ s yr}^{-1}$. However, a recent study by Qian et al. (2015) suggests that the rapid decrease in the orbital period is not true, and the new derived $O - C$ diagram shows a cyclic oscillation that may suggest that SDSS J001641-000925 is a triple system with a cool stellar companion with a mass of $M_3 \sin i' \sim 0.14 M_\odot$. Not coincidentally, the system 1SWASPJ234401.81-212229.1 was initially identified undergoing significant period decreases on the basis of the first 4 yr of SuperWASP observations (Lohr et al. 2012); however, further observations showed that the quadratic fit is part of the sinusoidal variation in the orbital period (Lohr et al. 2013a). This sinusoidal variation was argued in Lohr et al. (2013b) to be plausibly caused by a third body, which was then strongly supported by Koen (2014) on the basis of new multicolor photometry. A similar tertiary companion to the short-period contact binaries accounts for a large part of Table 6. It is known that the formation of this kind of contact binary is driven by angular momentum loss (AML) via magnetic braking and/or a tertiary companion. However, the timescales of the AML of

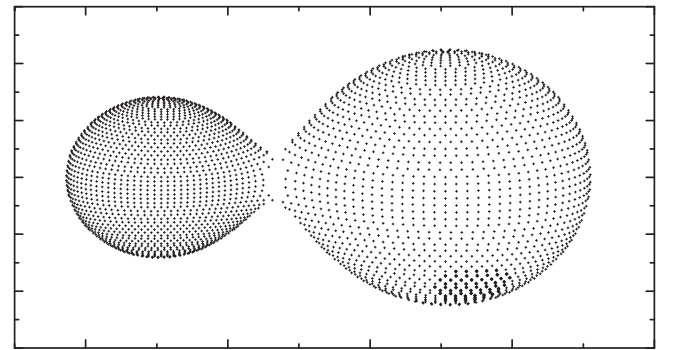


Figure 7. Geometrical structure of J074658 with a dark spot on the more massive component at phase 0.75 calculated with parameters listed in the fourth column of Table 5.

the magnetic braking are too long (Stepien 2006; Stępień 2011) to reach contact phase within the age of universe, so the tertiary companion may play an important role for the origin and evolution by extracting angular momentum from the central system (Qian et al. 2013, 2014, 2015; Zhu et al. 2010).

Of course, all of those conclusions and discussions are based on analysis of current photometric data. To support those results, especially the sinusoidal variation in the orbital period and a reliable mass ratio, as well as other related parameters, further observations including photometric and spectroscopic observations are urgently needed. Therefore, J074658 will remain in our observation plans. In addition, some other similar system will join to the list to enrich the sample database of short-period binaries.

This work is supported by the Chinese Natural Science Foundation (grant No. 11133007 and 11325315), the Strategic Priority Research Program “The Emergence of Cosmological Structure” of the Chinese Academy of Sciences (grant No. XDB09010202), and the Science Foundation of Yunnan Province (grant No. 2012HC011 and 2013FB084). New CCD photometric observations of the system were obtained with the 1 m and 60 cm telescopes at the Yunnan Observatories and the 2.16 m and 85 cm telescopes at Xinglong station of the National Astronomical Observatories of China. Many thanks to Dr. Marcus Lohr for his kindly sending us eclipse timings and uncertainties of J074658 in the SuperWASP archive, which cover

a time span from 2006 to 2010, and providing substantial aid. The authors thank professor Andrew Norton at Astrophysics Education of Royal Astronomical Society for providing us the data of SuperWASP.

REFERENCES

- Becker, A. C., Bochanski, J. J., Hawley, S. L., et al. 2011, *ApJ*, 731, 17
- Cox, A. N. 2000, *Allen's Astrophysical Quantities* (4th ed.; New York: Springer)
- Davenport, J. R. A., Becker, A. C., West, A. A., et al. 2013, *ApJ*, 764, 62
- Elkhateeb, M. M., Saad, S. M., Nouh, M. I., & Shokry, A. 2014, *NewA*, 28, 85
- Essam, A., Djurašević, G., Ahmed, N. M., & Jurković, M. 2014, *NewA*, 32, 16
- Jiang, D., Han, Z., Ge, H., Yang, L., & Li, L. 2012, *MNRAS*, 421, 2769
- Koen, C. 2014, *MNRAS*, 441, 3075
- Köse, O., Kalomeni, B., Keskin, V., Ulaş, B., & Yakut, K. 2011, *AN*, 332, 626
- Linnell, A. P., & Olson, E. C. 1989, *ApJ*, 343, 909
- Lohr, M. E., Norton, A. J., Kolb, U. C., et al. 2012, *A&A*, 542, A124
- Lohr, M. E., Norton, A. J., Kolb, U. C., et al. 2013a, *A&A*, 549, A86
- Lohr, M. E., Norton, A. J., Kolb, U. C., & Boyd, D. R. S. 2013b, *A&A*, 558, A71
- Lohr, M. E., Hodgkin, S. T., Norton, A. J., & Kolb, U. C. 2014, *A&A*, 563, A34
- Nefs, S. V., Birkby, J. L., Snellen, I. A. G., et al. 2012, *MNRAS*, 425, 950
- Norton, A. J., Payne, S. G., Evans, T., et al. 2011, *A&A*, 528, A90
- Ochsenbein, F., Bauer, P., & Marcout, J. 2000, *A&AS*, 143, 23
- Pollacco, D. L., Skillen, I., Collier Cameron, A., et al. 2006, *PASP*, 118, 1407
- Pribulla, T., Rucinski, S. M., Conidis, G., et al. 2007, *AJ*, 133, 1977
- Qian, S. 2002, *MNRAS*, 336, 1247
- Qian, S.-B., Jiang, L.-Q., Fernández Lajús, E., et al. 2015, *ApJL*, 798, L1
- Qian, S.-B., Liu, N.-P., Li, K., et al. 2013, *ApJS*, 209, 13
- Qian, S.-B., Wang, J.-J., Zhu, L.-Y., et al. 2014, *ApJS*, 212, 4
- Rucinski, S. M. 1992, *AJ*, 103, 960
- Rucinski, S. M., & Pribulla, T. 2008, *MNRAS*, 388, 1831
- Shengbang, Q. 2001, *Ap&SS*, 278, 415
- Stepien, K. 2006, *AcAau*, 56, 347
- Stepień, K. 2011, *AcAau*, 61, 139
- Van Hamme, W., & Wilson, R. E. 2007, *ApJ*, 661, 1129
- Wilson, R. E. 1979, *ApJ*, 234, 1054
- Wilson, R. E. 1990, *ApJ*, 356, 613
- Wilson, R. E. 2008, *ApJ*, 672, 575
- Wilson, R. E. 2012, *AJ*, 144, 73
- Wilson, R. E., & Devinney, E. J. 1971, *ApJ*, 166, 605
- Wilson, R. E., Van Hamme, W., & Terrell, D. 2010, *ApJ*, 723, 1469
- Yang, Y., & Liu, Q. 2003, *PASP*, 115, 748
- Yang, Y.-G., Lü, G.-L., Yin, X.-G., Zhu, C.-H., & Nakajima, K. 2009, *AJ*, 137, 236
- Yang, Y.-G., Wei, J.-Y., & Li, H.-L. 2010, *NewA*, 15, 155
- Zhang, X. B., Deng, L. C., Wang, K., et al. 2014, *AJ*, 148, 40
- Zhu, L., Qian, S.-B., Mikulášek, Z., et al. 2010, *AJ*, 140, 215
- Zhu, L.-Y., Qian, S.-B., Boonrucksar, S., He, J.-J., & Yuan, J.-Z. 2007, *ChJAA*, 7, 251
- Zhu, L. Y., Qian, S. B., Zola, S., & Kreiner, J. M. 2009, *AJ*, 137, 3574
- Zola, S., Gazeas, K., Kreiner, J. M., et al. 2010, *MNRAS*, 408, 464